


LEADERS: LEARNABLE DEEP RADIAL SUBSAMPLING FOR MRI RECONSTRUCTION

Zhiwen Wang¹  Bowen Li¹ Wenjun Xia¹ Chenyu Shen¹ Mingzheng Hou^{2,1} Hu Chen¹
Yan Liu³ Jiliu Zhou¹, Senior Member, IEEE Yi Zhang^{4,1,*}, Senior Member, IEEE

¹ College of Computer Science, Sichuan University, Chengdu 610065, China

²National Key Laboratory of Fundamental Science on Synthetic Vision, Sichuan University, Chengdu 610065, China

³College of Electrical Engineering, Sichuan University, Chengdu 610065, China

⁴School of Cyber Science and Engineering, Sichuan University, Chengdu 610065, China

ABSTRACT

Recently, deep learning approaches have shown great promise in learning MRI subsampling. The majority of existing works have focused on optimizing Cartesian or equipment-constrained Gaussian-like subsampling, ignoring the question of learning radial subsampling. This paper proposes a simple learnable radial subsampling technique for compressed sensing MRI. The proposed approach exploits a radial subsampling for direct estimation of all radial spokes' weights from radial sampling space. The proposed Learnable Deep Radial Subsampling (LEADERS) method can be easily integrated with any deep learning-based reconstruction algorithm. This method can provide reliable estimates in a deep learning manner. The effectiveness of the generated radial subsampling patterns is verified on two deep learning-based reconstruction models, with a large-scale, publicly available brain MRI datasets for two downsampling factors ($R = 4$ and 8). The numerical and visual experiments demonstrate that the learned radial subsampling patterns can be applied for different deep learning reconstruction models with different subsampling rates, and shows more efficient and effective results than the ones reconstructed using existing handcrafted radial subsampling patterns.

Index Terms— Deep learning, radial trajectory, learnable radial sampling, MRI, compressed sensing

1. INTRODUCTION

Magnetic resonance imaging (MRI) serves as an important non-invasive imaging modality for clinical diagnosis and biomedical research. However, MRI suffers from a relatively long acquisition time, which limits its sphere of application and probably discomfort the patients.

One way to speed up MR imaging is to observe partial measurement and reconstruct image using compressed sensing (CS) [1]. Unlike the Cartesian, radial subsampling methods, such as radial lines and Periodically Rotated Overlapping

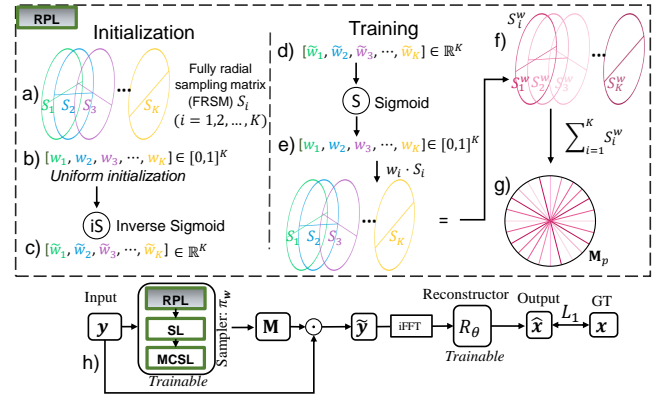


Fig. 1. Pipeline of our proposed LEADERS.

Parallel Lines with Enhanced Reconstruction (PROPELLER) [2], is relatively insensitive to motion artefacts due to the non-unique frequency-and-phase-encode directions and over-sampling of the over center position in k -space. Usually, these lines are empirically arranged without considering the scanning objects and reconstruction algorithms. However, separately designing sampling patterns and reconstruction methods would make the reconstructed images suboptimal [3].

An established practice to overcome the above issue is to employ a subsampling learning strategy to learn an optimal subsampling from a specific dataset for reconstruction methods [4]. This kind of method aims to optimize the sampling pattern to match the subsampled measurements with the target image that estimated via a reconstruction model. Compared to empirically designed subsampling patterns, e. g., variable density [5] and gold angle [6], massive deep learning-based efforts are made to this issue: 1) non-differentiable learning, such as reinforcement learning (RL) methods [7] that enable better Cartesian sampling selection, but may yield a mismatched subsampling pattern, that trained by a preset fixed subsampler and pretrained reconstructor; and 2) differential manners [4, 8] that work well for learning a Cartesian and

Gaussian-like subsampling subsampler optimized by gradients. However, these methods are limited to non-radial subsampling.

In this paper, we propose a novel sampling learning framework, named LEARNable DEep Radial Subsampling (LEADERS), which optimizes the radial line pattern and reconstructor jointly in an end-to-end manner for CS-MRI. To the best of our knowledge, this is the first attempt to learn radial subsampling patterns, which is trained with deep-learning-based reconstruction model jointly in a data driven fashion. We believe it has a huge potential for radial scenarios, which can be easily implemented by current MRI scanners. We show that the optimized subsampling pattern leads better imaging quality than traditional radial subsampling pattern in both qualitative and quantitative aspects.

2. METHOD

In this section, we first formulate CS-MRI problems from subsampled measurements. Then we describe the proposed network architecture. The overall pipeline of LEADERS is illustrated in Fig. 1.

2.1. MRI Reconstruction

Let $\mathbf{x} \in \mathbb{C}^{M \times N}$ denotes the image to be reconstructed and $\mathbf{M} \in \{0, 1\}^{M \times N}$ represents the Boolean subsampling pattern. The forward model of CS-MRI can be formulated as:

$$\tilde{\mathbf{y}} = \mathbf{M} \odot \mathbf{y} = \mathbf{M} \odot \mathcal{F}(\mathbf{x}) \quad (1)$$

where $\mathbf{y} \in \mathbb{C}^{M \times N}$ represents the fully sampled complex valued k -space data and $\tilde{\mathbf{y}}$ denote the subsampled measurements. \mathcal{F} stands for the discrete fast Fourier transform (FFT) and \odot denotes Hadamard product.

A reconstructed result contaminated by heavy artifacts, $\tilde{\mathbf{x}}$ called *zero-filling* image, can be obtained by directly applying the inverse FFT (iFFT) on $\tilde{\mathbf{y}}$, of which unobserved measurements are filled by zeros: $\tilde{\mathbf{x}} = \mathcal{F}^{-1}(\tilde{\mathbf{y}})$. To improve the imaging quality, iterative reconstruction (IR) method is also a popular choice, which usually introduces prior knowledge and formulates the reconstruction as an optimization problem. The main drawbacks of IR lie in three points: 1) handcrafted regularization term; 2) laborious parameter tuning; and 3) heavy computational cost. Since deep learning (DL)-based reconstruction can avoid these problems of IR and derive a joint optimization with subsampling pattern, we solve CS-MRI based on DL as:

$$\theta^* = \arg \min_{\theta} \mathbb{E}_{\mathbf{x}} [R_{\theta}(\tilde{\mathbf{y}}, \mathbf{x})] \quad (2)$$

where $R_{\theta}(\cdot)$ is a reconstruction network and θ denotes the parameter set of network. The goal of Eq. (2) is to minimize the error between reconstructed image and fully-sampled image.

2.2. Radial Sampler

As shown in Fig. 1, Radial Sampler (RS), $\pi_{\mathbf{w}}(\cdot)$, provides the learnable radial subsampling \mathbf{M} in our LEADERS framework. In this work, we construct RS following the effective differentiable learning [9, 10]. The goal of learnable radial subsampling with a reconstructor can be represented as:

$$\theta^*, \mathbf{w}^* = \arg \min_{\theta, \mathbf{w}} \mathbb{E}_{\mathbf{x}} [R_{\theta}(\tilde{\mathbf{y}}, \mathbf{x}) + \alpha \|\pi_{\mathbf{w}}(\mathbf{x})\|_1] \quad (3)$$

where \mathbf{w} denote the learnable weights of radial lines, $\|\cdot\|_1$ denotes the L_1 norm, and α is the sampling ratio. As shown in Fig. 1 h), RS consists of three cascaded layers, i.e., radial parameter layer (RPL), scaling layer (SL), and Monte Carlo searching layer (MCSL). In the following subsections, we elaborate these layers.

2.2.1. RPL

While designing RS, we simulate the gridding process with line drawing algorithm for simplicity and we ignore the convolutional interpolation and resampling to grid. RPL is initialized by the inverse *Sigmoid* function as:

$$\tilde{\mathbf{w}} = -\log\left(\frac{1}{\mathbf{w} - 1}\right)/s_1 \quad (4)$$

where $\tilde{\mathbf{w}} \in \mathbb{R}^K$, s_1 controls the inverse slope of the input \mathbf{w} [4], and the learnable weights \mathbf{w} are initialized with a uniform distribution $\mathbf{w} \sim U(0, 1)$, with K indicating the number of spokes covering the whole k -space grid with size of $M \times N$. In this period, as showed in Fig. 1 a)-c), RPL needs to build a fully radial sampling matrix (FRSM) $S_i \in \{0, 1\}^{M \times N}$ for fast mapping learnable weights to radial angles, and the subscript, $i = 1, 2, \dots, K$, is the spoke counter, where S_i means a spoke. In the FRSM, the angle between neighboring spokes is increased by a fixed step $\Delta\phi = \frac{180}{K}$.

In the period of forward inference, as showed in Fig. 1 d)-g), RPL outputs a probabilistic matrix $\mathbf{M}_p \in \mathbb{R}^{M \times N}$ for radial sampling. Let $\delta_{s_1}(\cdot)$ denotes the *Sigmoid* function with slope s_1 , $\mathbf{w} = \delta_{s_1}(\tilde{\mathbf{w}})$, and the forward computation of RPL is defined as:

$$\mathbf{M}_p = \begin{cases} \frac{1}{K} \sum_{i=1}^K w_i \cdot S_i, & \text{if } \sum_{i=1}^K w_i \cdot S_i \geq 1, \\ \sum_{i=1}^K w_i \cdot S_i, & \text{otherwise.} \end{cases} \quad (5)$$

where $w_i = \delta_{s_1}(\tilde{w}_i)$. The purpose of Eq. 5 is to map the weight w_i to the corresponding radial line S_i .

2.2.2. SL

Since \mathbf{M}_p cannot reflect the sampling ratio α , it is necessary to scale \mathbf{M}_p to \mathbf{M}_s , which can work at a given sampling ratio, i.e., $\frac{\|\mathbf{M}_s\|_1}{M \times N} = \alpha$. We follow LOUPE [4] to scale \mathbf{M}_p as:

$$\mathbf{M}_s = \begin{cases} \frac{\alpha}{\bar{m}} \mathbf{M}_p, & \text{if } \bar{m} \geq \alpha, \\ 1 - \frac{1-\alpha}{1-\bar{m}} (\mathbf{1} - \mathbf{M}_p), & \text{otherwise.} \end{cases} \quad (6)$$

where $\overline{m} = \frac{\|\mathbf{M}_p\|_1}{M \times N}$ and $\mathbf{M}_s \in [0, 1)^{M \times N}$.

2.2.3. MCSL

The Monte Carlo searching layer is also implemented following LOUPE [4] as a searching strategy. MCSL performs searching randomly in the FRSM as:

$$\mathbf{M} = \delta_{s_2}(\mathbf{M}_s - \mathbf{M}_{MC}) \quad (7)$$

where $\mathbf{M}_{MC} \sim U(0, 1)$ is a Monte Carlo searching matrix and $\delta_{s_2}(\cdot)$ denotes the *Sigmoid* function with slope s_2 .

2.3. Reconstruction Network

In the context of CS medical imaging, a large body of DL-based works has exerted great effort to tackle this ill-posed problem [11, 12, 13, 14, 15]. Unet [16], which was originally proposed for medical image segmentation, has shown impressive results in the field of image reconstruction. As a result, Unet is employed as the reconstruction network in our LEADERS framework. For simplicity, L_1 loss is used as the reconstruction loss:

$$\mathcal{L}^{Recon} = \|R_\theta(\mathcal{F}^{-1}(\mathbf{M} \odot \mathcal{F}(\mathbf{x}))) - \mathbf{x}\|_1 \quad (8)$$

3. RESULTS AND DISCUSSION

In this section, the proposed LEADERS is validated on a single-coil T1 MRI reconstruction task. In addition, we compared Unet and a recent DL-based state-of-the-art methods with different radial subsampling patterns.

Experiments were conducted on the emulated single-coil (ESC) fastMRI Brain [17] k -space data, remade by [18]. It is noticed that on the fastMRI challenge leaderboards, the difference between the results with 20% of the training set and the full training set is negligible. Meanwhile, our goal is not to competition to get better evaluation indicators, but instead, to search a learnable radial subsampling pattern in a certain dataset. Based on the above considerations, 500 and 80 volumes were selected from the whole fastMRI Brain (ESC) training/validation dataset, respectively. We used a total of 8000 fully sampled slices for training and 1280 slices for validation. No overlap between training and test dataset. As our model is differentiable, it is difficult to get it binary sampling pattern at once. A two-stage training strategy is adopted: 1) we first train the sampler RS with continuous sampling pattern \mathbf{M} and reconstruction network using the L_1 loss on the subsampled image for 500 epochs; and 2) then we fix RS, binarize \mathbf{M} , and finetune the reconstruction network.

Our method was implemented with PyTorch 1.7 using an NVIDIA RTX 8000 GPU with 48GB memory. Adam optimizer was adopted and the learning rate was set to 5×10^{-4} for whole networks. Since there is only L^{Recon} in the proposed model as formulated in Eq. (8), our proposed RS is an

unsupervised learning based network. The slopes of the logit values in RS were set as $s_1 = 5$ and $s_2 = 10$ for all experiments. We denote R is acceleration factor, which is defined as $R = 100/\alpha$.

In our experiments, we compared our method with other radial sampling methods using peak signal-to-noise ratio (PSNR).

Several popular radial subsampling patterns, including equiangular (\mathbf{M}_E), golden-angle [6] (\mathbf{M}_G), and random (\mathbf{M}_R) sampling were compared. Furthermore, to evaluate the impact of different reconstruction networks, both Unet [16] and MD-Recon-Net [19] (a recently proposed dual-domain reconstruction network) were employed.

Two representative visual results reconstructed with two different radial acceleration factors ($4\times$ and $8\times$) in Figs. 2 a) and b) help us better understand the quantitative results. In addition, the radial subsampling patterns generated using LEADERS and other handcrafted patterns are shown in Fig. 3. For each acceleration factor, the first row contains the reconstructed images using LEADERS and Unet with different subsampling patterns, and the second row shows the ground truth and the results reconstructed by MD-Recon-Net [19] with different subsampling patterns. It must mention that the result reconstructed by LEADERS means both subsampling pattern and reconstruction network (Unet) are trained jointly. The results marked as w/ \mathbf{M}_L in second column are obtained only training the reconstruction network (Unet or MD-Recon-Net) with the learned subsampling pattern from LEADERS. Figs. 2 a) and b) show that most methods are able to suppress the artifacts to varying degrees. At $4\times$ acceleration factor, the merit originated from the learned pattern from LEADERS is noticeable. Some details of gray matter are distorted, except in the results of LEADERS and the methods with \mathbf{M}_L . When the acceleration factor becomes high, the visual quality of LEADERS and the reconstructors with \mathbf{M}_L still outperform other methods in terms of both detail preservation and artifact suppression. The magnified parts in Figs. 2 a) and b) support this observation. In addition, the results reconstructed by MD-Recon-Net with the learned radial pattern using our proposed LEADERS illustrates the potential generalization ability of our method.

The quantitative comparisons on fastMRI test dataset with different sampling patterns at both acceleration factors are listed in Tab. 1. It can be noticed that the proposed LEADERS and two reconstructors with \mathbf{M}_L perform favorably against existing sampling patterns, which are consistent with our visual inspection.

4. CONCLUSION

In this paper, we introduce a learnable radial sampling technique, based on differentiable weights and Monte Carlo searching, that significantly improves the performance of radial methods for CS-MRI. We compare our method with

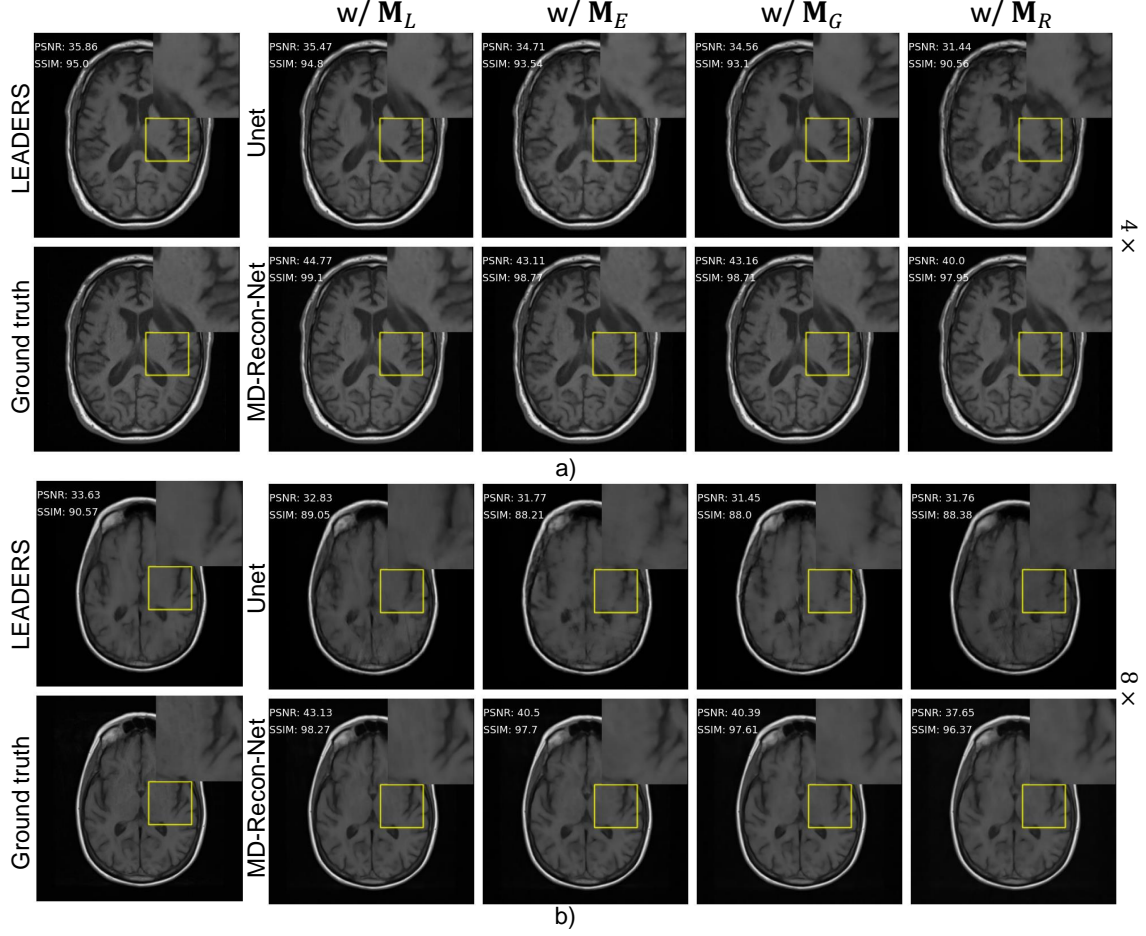


Fig. 2. A visual comparison of different radial subsampling patterns with two reconstructors at a) 4x and b) 8x acceleration factors. Zoom in to see the details.

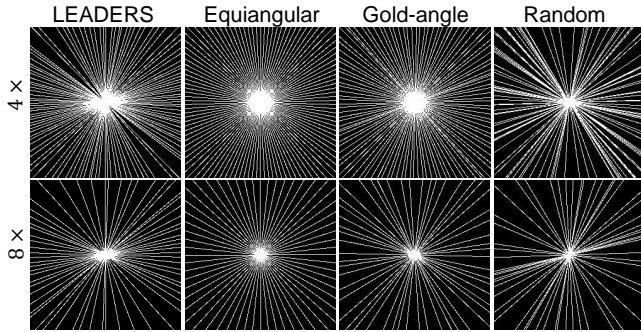


Fig. 3. Radial subsampling patterns generated using LEADERS and other handcrafted patterns.

Table 1. Quantitative results with two acceleration factors

| R | Model | Radial subsampling patterns | | | |
|-----|-----------|-----------------------------|----------------|----------------|----------------|
| | | \mathbf{M}_L | \mathbf{M}_E | \mathbf{M}_G | \mathbf{M}_R |
| | | PSNR | PSNR | PSNR | PSNR |
| 4x | Unet [16] | 35.03 | 34.14 | 33.76 | 32.91 |
| | MDR [19] | 42.41 | 40.50 | 40.49 | 38.42 |
| | Our | 35.73 | - | - | - |
| 8x | Unet [16] | 39.55 | 38.97 | 39.03 | 35.31 |
| | MDR [19] | 47.02 | 46.46 | 46.01 | 42.87 |
| | Our | 40.31 | - | - | - |

MDR: MD-Recon-Net

several popular radial sampling patterns on the fastMRI Brain dataset, outperforming them on both acceleration factors and stitching the gap between sampler and reconstructor with deep learning in terms of both qualitative and quantitative results. To the best of our knowledge, this is the first attempt to

design a radial subsampling pattern based on deep learning. Furthermore, we demonstrate the proposed method is generic to reconstruction models and robust at different acceleration factors.

5. COMPLIANCE WITH ETHICAL STANDARDS

This research study was conducted retrospectively using human subject data made available in open access by [17, 18]. Ethical approval was not required as confirmed by the license attached with the open access data.

6. CONFLICTS OF INTEREST

The authors declare that they have no conflicts of interest.

7. ACKNOWLEDGEMENTS

This work was supported in part by the National Natural Science Foundation of China under Grant 61871277, Grant 61902264, and Grant 61671312 and in part by the Sichuan Science and Technology Program under Grant 2021JDJQ0024 and Grant 2019YFS0125.

8. REFERENCES

- [1] D.L. Donoho, “Compressed sensing,” *IEEE Trans. Inf. Theory*, vol. 52, no. 4, pp. 1289–1306, 2006.
- [2] J.G. Pipe, “Motion correction with propeller mri: application to head motion and free-breathing cardiac imaging,” *Magn. Reson. Med.*, vol. 42, no. 5, pp. 963–969, 1999.
- [3] H.V. Grop et al., “Active deep probabilistic subsampling,” in *ICML*. PMLR, 2021, pp. 10509–10518.
- [4] C.D. Bahadir et al., “Deep-learning-based optimization of the under-sampling pattern in mri,” *IEEE Trans. Comput. Imag.*, vol. 6, pp. 1139–1152, 2020.
- [5] Z.M. Wang et al., “Variable density compressed image sampling,” *IEEE Trans. Image Process.*, vol. 19, no. 1, pp. 264–270, 2009.
- [6] S. Winkelmann et al., “An optimal radial profile order based on the golden ratio for time-resolved mri,” *IEEE Trans. Med. Imaging*, vol. 26, no. 1, pp. 68–76, 2006.
- [7] L. Pineda et al., “Active mr k-space sampling with reinforcement learning,” in *MICCAI*. Springer, 2020, pp. 23–33.
- [8] T. Yin et al., “End-to-end sequential sampling and reconstruction for mr imaging,” *arXiv preprint arXiv:2105.06460*, 2021.
- [9] E. Jang et al., “Categorical reparameterization with gumbel-softmax,” *arXiv preprint arXiv:1611.01144*, 2016.
- [10] C.J. Maddison et al., “The concrete distribution: A continuous relaxation of discrete random variables,” *arXiv preprint arXiv:1611.00712*, 2016.
- [11] H. Chen et al., “Low-dose ct with a residual encoder-decoder convolutional neural network,” *IEEE Trans. Med. Imaging*, vol. 36, no. 12, pp. 2524–2535, 2017.
- [12] M.S. Ran et al., “Denoising of 3d magnetic resonance images using a residual encoder–decoder wasserstein generative adversarial network,” *Med. Image. Anal.*, vol. 55, pp. 165–180, 2019.
- [13] H. Chen et al., “Learn: Learned experts’ assessment-based reconstruction network for sparse-data ct,” *IEEE Trans. Med. Imaging*, vol. 37, no. 6, pp. 1333–1347, 2018.
- [14] W.J. Xia et al., “Magic: Manifold and graph integrative convolutional network for low-dose ct reconstruction,” *IEEE Trans. Med. Imaging*, 2021.
- [15] W.J. Xia et al., “Ct reconstruction with pdf: Parameter-dependent framework for data from multiple geometries and dose levels,” *IEEE Trans. Med. Imaging*, 2021.
- [16] O. Ronneberger et al., “U-net: Convolutional networks for biomedical image segmentation,” in *MICCAI*. Springer, 2015, pp. 234–241.
- [17] J. Zbontar et al., “fastmri: An open dataset and benchmarks for accelerated mri,” *arXiv preprint arXiv:1811.08839*, 2018.
- [18] P.F. Guo et al., “Multi-institutional collaborations for improving deep learning-based magnetic resonance image reconstruction using federated learning,” in *CVPR*, 2021, pp. 2423–2432.
- [19] M.S. Ran et al., “Md-recon-net: A parallel dual-domain convolutional neural network for compressed sensing mri,” *IEEE Trans. Radiat. Plasma Med. Sci.*, vol. 5, no. 1, pp. 120–135, 2020.